

Excitations in a spin-polarized two-dimensional electron gas

Dominik Kreil, Raphael Hobbiger, Jürgen T. Drachta, and Helga M. Böhm
Institut für Theoretische Physik, Johannes Kepler Universität, 4040 Linz, Austria

A remarkably long-lived spin plasmon may exist in two-dimensional electron liquids with imbalanced spin up and spin down population. Predictions for this interesting mode by Agarwal *et al.* [Phys. Rev. B **90**, 155409 (2014)] are based on the random phase approximation. We here show how to account for spin dependent correlations from known ground state pair correlation functions and study the consequences on the various spin dependent longitudinal response functions. The spin plasmon dispersion relation and its critical wave vector for Landau damping by minority spins turn out to be significantly lower. We further demonstrate that spin dependent effective interactions imply a rich structure in the excitation spectrum of the partially spin-polarized system. Most notably, we find a “magnetic antiresonance”, where the imaginary part of both, the spin-spin as well as the density-spin response function vanish. The resulting minimum in the double-differential cross section is awaiting experimental confirmation.

PACS numbers: 73.22.Lp, 73.21.b, 73.20.Mf, 72.25.b

I. INTRODUCTION

In non-magnetic electron layers, (*i.e.* with vanishing spin-polarization $P \equiv (N_\uparrow - N_\downarrow)/N$, total number of particles $N = N_\uparrow + N_\downarrow$, and N_σ being the number of electrons with spin up or down), collective spin modes rapidly decay into electron-hole pairs. For spin-polarized systems, however, as was convincingly demonstrated by Agarwal *et al.*¹, the Random Phase Approximation (RPA) yields an amazingly long-lived spin plasmon. This “longitudinal magnon” exists, *inside* the band of electron-hole pairs with the majority spin, up to a critical wave vector $q_{\text{spl}}^{\text{max}}$ before decaying rapidly into electron-hole pairs of the minority spin population.

In this report we show, among other results, that going beyond the traditional RPA leads to much lowered critical wave vectors. For both, the conventional plasmon as well as the spin plasmon, this effect becomes more pronounced for dilute systems, where correlations play an important role.

Experiments^{2,3} on heterostructures were performed on the conventional plasmon (*i.e.* the $P = 0$ charge plasmon) for areal densities $n = 1.9 \times 10^{13} \text{ cm}^{-2}$ and $n = (0.77 \dots 4) \times 10^9 \text{ cm}^{-2}$. This corresponds to Wigner-Seitz radii $r_s \lesssim 2$ and $r_s \approx 10 \dots 20$, respectively (as usual, $r_s \equiv 1/(a_B^* \sqrt{\pi n})$ with a_B^* being the material’s effective Bohr radius). The influence of electron correlations on the dispersion can be estimated using the simulation based⁴ charge-charge response function from Ref. 5. At the coupling parameters of interest, as shown in Table I, the critical wave vector $q_{\text{pl}}^{\text{max}}$ for Landau damping changes by typically $\geq 20\%$. Only in systems of sufficiently low r_s and for low wave vectors q the mode can be detected near the RPA result. Possible candidates for such dense systems could be electron gases near a SrTiO₃ surface^{6–10} with a high background dielectric constant ϵ_b ; (however, anisotropy effects need to be accounted for, too¹¹).

For the spin plasmon, we here show that spin dependent correlations pull this mode down drastically towards the minority particle-hole band. Consequently, it ap-

pears questionable whether this excitation can be resolved experimentally, even if it may stay slightly above the boundary. We also give results for low densities and predict a new phenomenon.

In Sec. II we briefly describe the theory. We first introduce our method to account for spin dependent correlations via effective (static) interactions¹², and then study the consequences for the various response functions. In Sec. III we critically discuss our results. Special emphasis is put on the critical wave vector for Landau damping of the charge plasmon and a detailed investigation of the spin plasmon. Finally, we present a hitherto unknown valley in the imaginary part of the longitudinal spin response, the “magnetic antiresonance”, and summarize our conclusions in Sec. IV.

II. THEORY

A. Spin dependent effective interactions

In RPA-type approaches the partial response functions $\chi_{\sigma\sigma'}$ forming the matrix χ are determined by the equation¹³

$$\chi^{-1}(q, \omega) = \chi^{0-1}(q, \omega) - \mathbf{V}(q) \quad . \quad (1)$$

Here, χ^0 contains the spin-resolved parts $\delta_{\sigma\sigma'} \chi_\sigma^0$ of Stern’s polarizability¹⁴, and \mathbf{V} the effective interactions $V_{\sigma\sigma'}$ between electrons of spin σ and σ' . (Eq. (1) may also be read as the definition¹⁵ of dynamic interactions $\mathbf{V}(q, \omega)$). In the bare RPA studied by Agarwal *et al.*¹ all $V_{\sigma\sigma'}$ are replaced with the Coulomb interaction, $v(q) = 2\pi e^2/(\epsilon_b q)$.

For a paramagnetic layer, *i.e.* $P=0$, various static approximations have been presented^{16–20}. Commonly, the effective spin dependent interactions are expressed via so-called „local field corrections”,

$$V_{\sigma\sigma'}(q) = v(q) (1 - G_{\sigma\sigma'}(q)) \quad . \quad (2)$$

We term approaches of type (2) ‘‘Generalized RPA’’ (GRPA).

The matrix equation (1) for χ reads explicitly (*c.f.* Eq. (1) of Ref. 1)

$$\begin{pmatrix} \chi_{\uparrow\uparrow} & \chi_{\uparrow\downarrow} \\ \chi_{\uparrow\downarrow} & \chi_{\downarrow\downarrow} \end{pmatrix}^{-1} = \begin{pmatrix} \chi_{\uparrow}^0 & 0 \\ 0 & \chi_{\downarrow}^0 \end{pmatrix}^{-1} - \begin{pmatrix} V_{\uparrow\uparrow} & V_{\uparrow\downarrow} \\ V_{\uparrow\downarrow} & V_{\downarrow\downarrow} \end{pmatrix}, \quad (3)$$

where we also invoked the symmetry $(\uparrow\downarrow) \leftrightarrow (\downarrow\uparrow)$.

As pointed out by E. Krotschek²¹, an essential requirement for a response function is to fulfill the first and zeroth moment sum rule. The latter invokes the spin-resolved static structure factors

$$S_{\sigma\sigma'}(q) \equiv \frac{1}{\sqrt{N_{\sigma}N_{\sigma'}}} \langle \delta\hat{n}_{\mathbf{q}\sigma} \delta\hat{n}_{-\mathbf{q}\sigma'} \rangle, \quad (4)$$

with the partial density fluctuation operator $\delta\hat{n}_{\mathbf{q}\sigma}$ and the prefactor convention of Gori-Giorgi et al.¹². Again, for non-interacting fermions, \mathbf{S}^0 , the matrix of static structure factors, is diagonal¹³. The full static structure factor is given by $S(q) = \sum_{\sigma\sigma'} S_{\sigma\sigma'}(q) \sqrt{n_{\sigma}n_{\sigma'}/n}$.

The pertinent sum rules then read

$$- \int_0^{\infty} \frac{d\omega}{\pi} \text{Im} \chi_{\sigma\sigma'}(q, \omega) = \sqrt{n_{\sigma}n_{\sigma'}} S_{\sigma\sigma'}(q), \quad (5a)$$

$$- \int_0^{\infty} \frac{d\omega}{\pi} \omega \text{Im} \chi_{\sigma\sigma'}(q, \omega) = \delta_{\sigma\sigma'} n_{\sigma} \frac{\hbar q^2}{m}, \quad (5b)$$

(m being the effective electron mass due to the semiconductor background lattice).

In order to determine $V_{\sigma\sigma'}(q)$ from these conditions we replace, as a first step, $\chi_{\sigma\sigma'}^0$ in Eq. 5 with a single-pole (also called ‘‘collective’’) approximation²². This allows us to derive a compact expression relating the effective interactions with the spatial structure. Introducing the matrix $\bar{\mathbf{V}}$ of spin weighted interactions via $\bar{V}_{\sigma\sigma'}(q) \equiv \sqrt{n_{\sigma}n_{\sigma'}/n} V_{\sigma\sigma'}(q)$, we arrive at the matrix equation

$$\bar{\mathbf{V}}(q) = \frac{\hbar^2 q^2}{4mn} \left(\mathbf{S}^{-2}(q) - \mathbf{S}^{0-2}(q) \right). \quad (6)$$

Result (6) is the analogue of the particle-hole potential²¹ defined as

$$\bar{V}_{\text{ph}}(q) = \frac{\hbar^2 q^2}{4mn} \left(\frac{1}{S(q)^2} - \frac{1}{S^0(q)^2} \right). \quad (7)$$

The strength of this formula is to contain an approximate summation of both, ladder- and ring-diagrams, thus capturing important long- as well as short-ranged attributes²³. Spelling out Eq. (6) explicitly, we obtain

$$D(q) = S_{\uparrow\uparrow}(q) S_{\downarrow\downarrow}(q) - S_{\uparrow\downarrow}^2(q), \quad (8a)$$

$$\bar{V}_{\uparrow\downarrow}(q) = - \frac{\hbar^2 q^2}{4mn} \frac{S_{\uparrow\downarrow}(q) [S_{\uparrow\uparrow}(q) + S_{\downarrow\downarrow}(q)]}{D^2(q)}, \quad (8b)$$

$$\bar{V}_{\uparrow\uparrow}(q) = \frac{\hbar^2 q^2}{4mn} \left[\frac{S_{\downarrow\downarrow}^2(q) + S_{\uparrow\downarrow}^2(q)}{D^2(q)} - \frac{1}{S_{\uparrow}^0(q)^2} \right], \quad (8c)$$

and the analogous expression for $\bar{V}_{\downarrow\downarrow}$. These interactions can now be used in Eq. (3) to calculate the response functions from any given set of spin-resolved static structure factors $S_{\sigma\sigma'}(q)$.

Note that we do *not* calculate the response functions — neither the spin plasmon nor any other feature — within the above plasmon-magnon-pole approximation. The latter only served the purpose of obtaining suitable effective spin dependent interactions. As discussed in Ref. 23, Eq. (7) can be seen as the *definition* of an optimal static effective interaction if the ground state structure factor is known.

High quality spin-resolved ground state structure calculations were performed by Gori-Giorgi et al.¹². With reptation quantum Monte Carlo (QMC) techniques they obtained the pair-distribution functions $g_{\sigma\sigma'}(r)$. A Fourier transform yields the static structure factors we need:

$$S_{\sigma\sigma'}(q) = \delta_{\sigma\sigma'} + \sqrt{n_{\sigma}n_{\sigma'}} \int d^2r [g_{\sigma\sigma'}(r) - 1] e^{i\mathbf{q}\cdot\mathbf{r}}. \quad (9)$$

Naturally, all QMC data are limited in real space. Hence an extension $g_{\sigma\sigma'}(r \rightarrow \infty)$ is necessary in order to establish the proper long-wavelength behavior. Using reduced units $\bar{q} \equiv q/k_{\text{F}}$ where $k_{\text{F}} = \sqrt{2\pi n}$, and denoting spins opposite to σ as $\bar{\sigma}$, this limit reads¹²

$$S_{\sigma\sigma'}(\bar{q} \rightarrow 0) = \tilde{\xi}_{\sigma\sigma'} \frac{\bar{q}}{\pi} + \frac{\sqrt{n_{\sigma}n_{\sigma'}}}{n} \frac{\bar{q}^{3/2}}{2^{3/4} \sqrt{r_{\text{S}}}} + \mathcal{O}(\bar{q}^2),$$

$$\tilde{\xi}_{\sigma\sigma'} = \delta_{\sigma\sigma'} \sqrt{n_{\bar{\sigma}}/n_{\sigma}} - \delta_{\sigma\bar{\sigma}}. \quad (10)$$

For the spin-summed $g(r)$ at any P , as well as for the partial $g_{\sigma\sigma'}(r)$ at $P=0$ and $P=1$, analytical expressions are given in Ref. 12. These are based on skillful extrapolation to large r and we follow this procedure for the $P=0.48$ data²⁴. The delicate behavior of the effective interaction between minority spins, $V_{\downarrow\downarrow}(q)$, necessitates additional care with respect to ensuring the high-density (RPA) limit of the fit for all partial $S_{\sigma\sigma'}(q)$.

With these results for \mathbf{S} the effective interactions \mathbf{V} are now obtained from (6). This is then used in the matrix equation (3) to determine χ .

As a check, we evaluated the sum rules (5) for the spin-summed charge-charge response function. The f-sum rule (5b) is excellently fulfilled for all r_{s} , the input $S(q)$ is reproduced within a few percent of error.

B. Response functions

In an electron liquid subject to an electrostatic external potential V^{ext} and an uniaxial magnetic field \mathbf{B}^{ext} the induced partial spin densities δn_{σ} manifest themselves in the following observables: the induced particle density $\delta n = \delta n_{\uparrow} + \delta n_{\downarrow}$, the induced longitudinal magnetization proportional to $\delta s \equiv \delta n_{\uparrow} - \delta n_{\downarrow}$, and transverse magnetization components. The Pauli spin-flip operators govern the transverse linear response functions;

their eigenmodes are the "conventional" magnons of condensed matter physics. Longitudinal excitations are fully decoupled^{25,26}. Rescaling the magnetic field by Bohr's magneton and the g -factor, $b^{\text{ext}} \equiv g\mu_B|\mathbf{B}|^{\text{ext}}/2$, we have

$$\begin{pmatrix} \delta n \\ \delta s \end{pmatrix} = \begin{pmatrix} \chi_{nn} & \chi_{ns} \\ \chi_{ns} & \chi_{ss} \end{pmatrix} \cdot \begin{pmatrix} V^{\text{ext}} \\ b^{\text{ext}} \end{pmatrix}. \quad (11)$$

Apparently, in electron layers with imbalanced spin population a longitudinal magnetization can be induced either by a magnetic field or by an electrostatic potential (or both). The corresponding longitudinal magnon, *i.e.* the collective mode in the spin density δs at vanishing b^{ext} and V^{ext} is termed¹ "spin plasmon".

Decomposed into their spin-resolved contributions the relevant susceptibilities read

$$\chi_{nn} = \chi_{\uparrow\uparrow} + 2\chi_{\uparrow\downarrow} + \chi_{\downarrow\downarrow}, \quad (12a)$$

$$\chi_{ss} = \chi_{\uparrow\uparrow} - 2\chi_{\uparrow\downarrow} + \chi_{\downarrow\downarrow}, \quad (12b)$$

$$\chi_{ns} = \chi_{\uparrow\uparrow} - \chi_{\downarrow\downarrow}. \quad (12c)$$

They all share the same denominator Δ ,

$$\Delta = 1 - V_{\uparrow\uparrow}\chi_{\uparrow}^0 - V_{\downarrow\downarrow}\chi_{\downarrow}^0 + (V_{\uparrow\uparrow}V_{\downarrow\downarrow} - V_{\uparrow\downarrow}^2)\chi_{\uparrow}^0\chi_{\downarrow}^0. \quad (13)$$

For arbitrary spin-polarization P all $V_{\sigma\sigma'}$ differ. In the paramagnetic case the symmetry $V_{\uparrow\uparrow} = V_{\downarrow\downarrow}$ implies that

$$\Delta^{P=0} = 1 - V_{\uparrow\uparrow}(\chi_{\uparrow}^0 + \chi_{\downarrow}^0) + (V_{\uparrow\uparrow}^2 - V_{\uparrow\downarrow}^2)\chi_{\uparrow}^0\chi_{\downarrow}^0. \quad (14)$$

For spin independent interactions, as in the bare RPA, Eq. (13) reduces to

$$\Delta^{\text{RPA}} = 1 - v(\chi_{\uparrow}^0 + \chi_{\downarrow}^0) = \epsilon^{\text{RPA}}. \quad (15)$$

Obviously, the effective interactions change the collective excitations compared to their RPA behavior due to two distinct causes: The difference between like and unlike spins arising from the Pauli principle influences systems with arbitrary P : from Eq. (14) it is seen that a denominator of the type $1 - V\chi^0$ with *some* interaction $V(q)$ would require $V_{\uparrow\uparrow} = V_{\downarrow\downarrow}$, also for $P=0$. In addition, the substantially different screening between minority and majority components, manifest in $V_{\uparrow\uparrow} \neq V_{\downarrow\downarrow}$, gives rise to further modifications for spin-imbalanced systems.

For completeness, we also list the numerators involved in Eq. (12),

$$\chi_{ss}^{nn} = \frac{1}{\Delta} \left(\chi^0 - [V_{\uparrow\uparrow} + V_{\downarrow\downarrow} \mp 2V_{\uparrow\downarrow}]\chi_{\uparrow}^0\chi_{\downarrow}^0 \right), \quad (16a)$$

$$\chi_{ns} = \frac{1}{\Delta} \left(\chi_{\uparrow}^0 - \chi_{\downarrow}^0 + [V_{\uparrow\uparrow} - V_{\downarrow\downarrow}]\chi_{\uparrow}^0\chi_{\downarrow}^0 \right). \quad (16b)$$

We now turn to the numerical results of our approach.

III. RESULTS

A. Charge plasmon

We start with studying the critical wave vector $q_{\text{pl}}^{\text{max}}$ of the $P=0$ charge plasmon. This is insensitive to whether

using Eq. (6) or (7). Table I compares our data with those following from Ref. 5 based on simulations⁴ for $\omega=0$. Considering that, by contrast, $V_{\text{ph}}(q)$ arises from an

r_s	2	5	10	20	30	40
$n_{\text{GaAs}} [10^9 \text{ cm}^{-2}]$	75.2	12	3	0.75	0.33	0.19
	$q_{\text{pl}}^{\text{max}}$					
RPA [k_{F}^{-1}]	1.50	2.45	3.55	5.09	6.28	7.29
RPA [10^5 cm^{-1}]	10.3	6.75	4.88	3.50	2.88	2.51
	change from RPA					
GRPA - Ref. 5	-25%	-40%	-52%	-	-	-
GRPA - Eq. (7)	-15%	-37%	-50%	-62%	-68%	-71%

TABLE I. Paramagnetic charge plasmon critical wave vector. Upper two lines: (bare) RPA value in reduced units and for a GaAs quantum well. Lower two lines: Percental change due to the local field corrections of Davoudi *et al.*⁵ and with $G(q) = 1 - V_{\text{ph}}(q)/v(q)$ based on Monte Carlo $S(q)$ from Ref. 12.

ω -integration, it is striking how close the values are for $r_s \approx 5 \dots 10$. The discrepancy at small r_s is removed if $V_{\text{ph}}(q)$ is determined numerically from the sum rule (5a) without the single mode approximation. This strongly supports the quality of our approach. In the following we prefer to stick to the analytic relations (8) between the effective interactions and the static structure factors, in favor of better physical insight.

B. Spin plasmon

Concerning both, charge- and spin response, Fig. 1 compares the real and imaginary part of the denominator $\Delta(q, \omega)$ of the susceptibilities (12) with its RPA counterpart, $\epsilon^{\text{RPA}}(q, \omega)$. The same system parameters and wave vector are chosen as in Fig. 2a of Ref. 1. In the GRPA the typical "shark-fin" structure of the imaginary part is smoothed for the minority band and enhanced for the majority spins. Like in bare RPA, also for spin-sensitive effective interactions the real part of the denominator has an additional zero above the first band edge. This zero was identified in Ref. 1 as the spin plasmon and in careful investigations proven to be quite stable against damping by impurity scattering.

The spin plasmon, if a true collective mode and pole of χ_{ss} , can be obtained from either of the two equivalent requirements:

$$\text{Re } \Delta(q, \omega) = 0 \Leftrightarrow -\text{Im } \chi_{ss}(q, \omega) = \max. \quad (17)$$

Inside the particle-hole band of the minority spins the two routes do not yield exactly the same result. We follow Ref. 1 by determining the dispersion from the roots of $\text{Re } \Delta(q, \omega)$. Fig. 2 shows the numerically obtained zeros for $r_s=2$ and $P=0.48$ in the (q, ω) -plane. For comparison, the RPA and the single-mode result ("Bijl-Feynman type" or "BF")¹³ are displayed as well. The inset of Fig. 2 confirms that our spin dependent GRPA recovers the high density (*i.e.* RPA) limit.

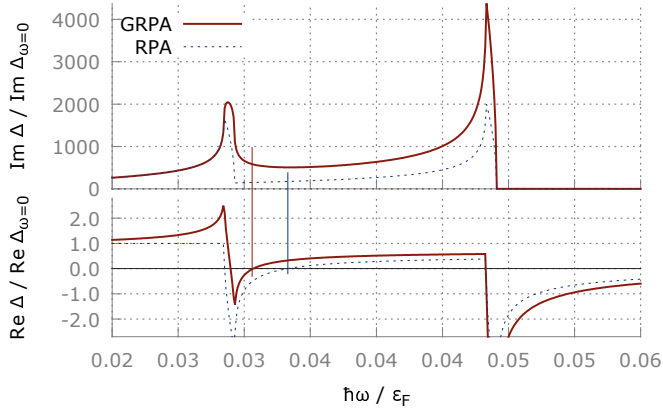


FIG. 1. Denominator of the spin response functions $\chi_{\sigma\sigma'}(q, \omega)$ for $r_s=2$, $q=0.02 k_F$, and polarization $P=0.48 \approx 0.5$ in bare RPA (dotted lines) and our GRPA (full curves). The upper (lower) panel gives the imaginary (real) part; the vertical lines mark the zeroes of the real part. Terms $\propto \chi_{\uparrow}^0 \chi_{\downarrow}^0$ as in Eq. (14) enter both, $\Delta(q, \omega)$ as well as the numerators of the $\chi_{\sigma\sigma'}$, changing the overall height of both. For better comparability, we thus rescale the curves.

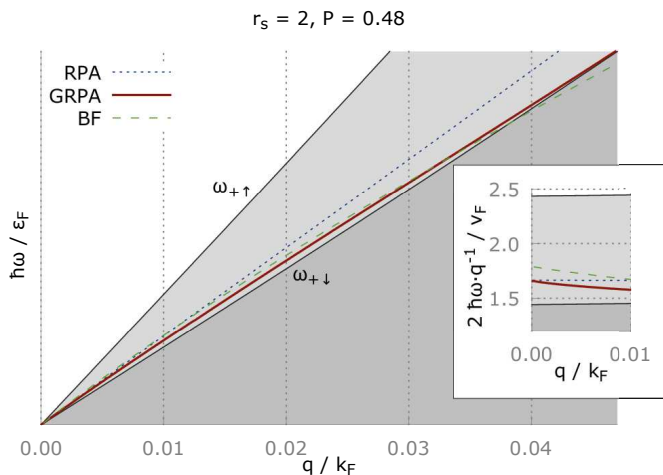


FIG. 2. Spin plasmon dispersion for $r_s=2$ and $P=0.48$ in bare RPA (blue dotted line), GRPA (with the effective interactions of Eq. (6), red solid line) and single-pole approximation (green dashed line). All three modes start in the continuum of the majority spins (light grey area). Our result enters the minority spin continuum (dark grey area) tangentially at a much lower $q_{\text{spl}}^{\text{max}}/k_F$ than that of the RPA. The inset shows the dispersion divided by the wave vector, demonstrating that our approach gives the same initial slope as the RPA.

It is seen that the inclusion of spin effects in the effective potentials $V_{\sigma\sigma'}$ lowers the spin plasmon’s position significantly. As the zero of $\text{Re } \Delta(q, \omega)$ is shifted towards lower frequencies, it is simultaneously moved closer to the “fin structure” which is smeared out by spin–correlation effects (*cf.* Fig. 1, upper part). In addition, the relative

height of $\text{Im } \Delta(q, \omega)$ is larger in the GRPA, implying that damping²⁷ of the mode is stronger everywhere. Both effects, the close vicinity to Landau damping by minority spins as well as the overall increase of $\text{Im } \Delta(q, \omega)$ heighten the challenge for experimentally verifying the position of this mode.

Since the spin plasmon, being an acoustic mode, is rather close to the relevant band edge for all q , its critical wave vector for Landau damping is much smaller than that of the charge plasmon. Consequently, while the effective interactions $V_{\sigma\sigma'}(q)$ appear rather unaffected by minor variations in $g_{\sigma\sigma'}(r \rightarrow \infty)$, the spin plasmon is quite sensitive to such changes. Reducing these uncertainties would require the exact $q^{>3/2}$ expansion coefficients of $S_{\sigma\sigma'}(q \rightarrow 0)$. In Fig. 3 we present our results for the critical wave vector $q_{\text{spl}}^{\text{max}}$, where the spin plasmon tangentially hits the band edge $\omega_{+\downarrow}$.

It is evident that exchange–correlation effects lower $q_{\text{spl}}^{\text{max}}$ to approximately one third of its RPA value. Even if we account for a substantial spread in the $q^{5/2}$ coefficient of $S_{\sigma\sigma'}(q \rightarrow 0)$, the reduction is still 50%. In order to reduce the uncertainty in the $r \rightarrow \infty$ input data high accuracy calculations of $S(q)$ in this regime are desirable (e.g. via the so-called “FHNC” method²⁸). Both, the RPA and the GRPA yield a nearly density independent critical wave vector beyond $r_s \gtrsim 10$, as it is typical for static effective interactions. Investigations in the dynamic many body approach²⁹ are under way. This holds the promise of a “charge plasmon revival”³⁰ at large wave vectors, as first observed in the pioneering work of Neilson *et al.*¹⁸.

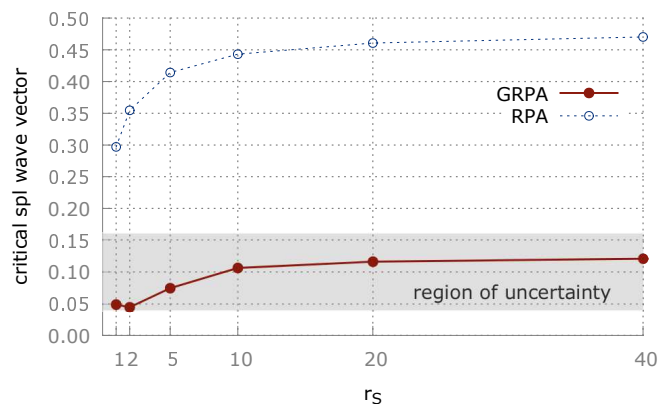


FIG. 3. Critical wave vector $q_{\text{spl}}^{\text{max}}(P=0.48)$ in our GRPA (red solid line) and bare RPA (blue dotted line) versus coupling strength. The shaded area is an estimate of the error induced by the limited r –range of the input Monte Carlo data¹².

C. Fermi Liquid parameters

At the densities of interest the Coulomb energy is at least of similar order as the kinetic energy. Nevertheless

the Fermi surface is remarkably robust, as captured by Landau's Fermi liquid theory^{25,31}. Low lying excitations behave like quasiparticles; their Fourier expanded interaction defines the Landau parameters (rescaled with the (true) density of states at the Fermi surface)^{32,33}

$$f_{\mathbf{k},\mathbf{k}'}^{\sigma,\sigma'} = \sum_{\ell} f_{\ell}^{\sigma,\sigma'} \cos(\ell\theta_{\mathbf{k},\mathbf{k}'}), \quad (18)$$

$$f_{\ell}^{\sigma,\sigma'} \equiv \frac{\hbar^2 \pi}{m^*} F_{\ell}^{\sigma,\sigma'} = \frac{m}{m^*} \frac{\epsilon_F}{n} F_{\ell}^{\sigma,\sigma'}. \quad (19)$$

At $P=0$ the spin-symmetric and -antisymmetric $\ell=0, 1$ combinations $F_{\ell}^{\text{S},\text{a}} \equiv \frac{1}{2}(F_{\ell}^{\uparrow\uparrow} \pm F_{\ell}^{\uparrow\downarrow})$ yield the effective mass m^* , the compressibility κ and the spin-susceptibility. These are, in turn, related to the long wavelength behavior of the effective interactions. An example is^{32,34}

$$\begin{aligned} \frac{\kappa^0}{\kappa} &= \frac{m}{m^*} (1 + F_0^{\text{S}}) = \frac{1 + F_0^{\text{S}}}{1 + \frac{1}{2}F_1^{\text{S}}}, \\ 1 - \frac{\kappa^0}{\kappa} &= \frac{nv(q)}{\epsilon_F} G^{\text{S}}(q \rightarrow 0), \end{aligned} \quad (20)$$

with the $P=0$ local field corrections $G^{\text{S}} \equiv (G_{\uparrow\uparrow} + G_{\uparrow\downarrow})/2$, and κ^0 is the compressibility of free Fermions. Detailed studies of quasiparticles in spin-imbalanced systems are beyond the scope of this work. It appears interesting, however, to study the slope of our spin dependent local field corrections.

Following Iwamoto³² in defining $\kappa^0/\kappa \equiv 1 + F^{\text{S}}$, we investigate the Landau-like parameters

$$\begin{aligned} F_{\sigma\sigma'} &\equiv -\frac{n}{\epsilon_F} \lim_{q \rightarrow 0} v(q) G_{\sigma\sigma'}(q) \\ &= \frac{n}{\epsilon_F} \lim_{q \rightarrow 0} [V_{\sigma\sigma'} - v(q)]. \end{aligned} \quad (21)$$

Having ensured the long wave length limit (10) of the static structure factors, the effective potentials (8) imply

$$F_{\uparrow\uparrow} = \frac{\pi^2}{8} (1-P)^2 - \frac{\pi^2}{4}, \quad (22a)$$

$$F_{\downarrow\downarrow} = \frac{\pi^2}{8} (1+P)^2 - \frac{\pi^2}{4}, \quad (22b)$$

$$F_{\uparrow\downarrow} = \frac{\pi^2}{8} (P^2 - 1). \quad (22c)$$

Consequently, the combination $F^{\text{a}} \equiv F_{\downarrow\downarrow} + F_{\uparrow\uparrow} - 2F_{\uparrow\downarrow}$ vanishes for any P . Thus the initial slope of the spin plasmon is not altered compared to the RPA result¹, as also evident from Fig. 2. Without additional knowledge, more accurate values of $F_{\sigma\sigma'}$ must remain uncertain³⁵.

D. Magnetic antiresonance

We conclude our studies by presenting results for dilute systems. Knowing the distinct behavior of the various response contributions $\chi_{\sigma\sigma'}$ allows the identification of different (q, ω) -regions of interest for the imaginary parts of χ_{nn} , χ_{ss} and χ_{ns} , respectively. Table II shows a comparison of the most prominent cases.

For vanishing $\uparrow\downarrow$ contributions, density-wave excitations have the same magnitude as spin-fluctuations;

contributions to each fluctuating component $\delta n_{\mathbf{q},\sigma} = \chi_{\sigma\sigma} V^{\text{ext}}$ arise solely from identical spins, the two δn_{σ} react quasi independently. If also $\chi_{\uparrow\uparrow}$ vanishes, the whole excitation arises from the minority spins and the system behaves like a ferromagnetic one.

Condition	Consequence
$\text{Im}\chi_{\uparrow\downarrow}=0$	$\text{Im}\chi_{nn} = \text{Im}\chi_{ss}$
$\text{Im}\chi_{\uparrow\downarrow}=\text{Im}\chi_{\uparrow\uparrow}=0$	$\text{Im}\chi_{nn} = \text{Im}\chi_{ss} = -\text{Im}\chi_{ns} = \text{Im}\chi_{\downarrow\downarrow}$
$\text{Im}\chi_{\uparrow\uparrow}=\text{Im}\chi_{\downarrow\downarrow}$	$\text{Im}\chi_{nn} = 2 \text{Im}(\chi_{\uparrow\uparrow} + \chi_{\uparrow\downarrow})$
	$\text{Im}\chi_{ss} = 2 \text{Im}(\chi_{\uparrow\uparrow} - \chi_{\uparrow\downarrow})$
	$\text{Im}\chi_{ns} = 0$
$\text{Im}\chi_{\uparrow\downarrow} = \begin{cases} \text{Im}\chi_{\uparrow\uparrow} \\ \text{Im}\chi_{\downarrow\downarrow} \end{cases}$	$\text{Im}\chi_{nn} = 4 \text{Im}\chi_{\uparrow\uparrow}$
	$\text{Im}\chi_{ss} = 0$
	$\text{Im}\chi_{ns} = 0$

TABLE II. Specific excitation regimes and their requirements. Fig. 4 compares all these loss functions for one characteristic q -value as function of frequency.

In partially spin-polarized systems, at (q, ω) -values with $\text{Im}\chi_{\uparrow\uparrow} = \text{Im}\chi_{\downarrow\downarrow}$, the excitation spectrum is qualitatively the same as for the paramagnetic case.

Furthermore, a totally new structure emerges in the majority particle-hole band: The imaginary part of χ_{ss} vanishes exactly along a line $\omega_{\text{MAR}}(q)$ and stays very small in its neighborhood. Before discussing this in more detail, we compare the imaginary parts of the various response functions in Fig. 4 to identify the excitation regimes given in Table II.

First, we observe that all three *partial* response functions behave very similar throughout the region $\hbar\omega \lesssim 4.2 \epsilon_F$, leading, however, to significant differences in the spin summed response functions. In this range the imaginary part of the spin-spin response function $\text{Im}\chi_{ss}$ dominates over $\text{Im}\chi_{nn}$ and $\text{Im}\chi_{ns}$. Second, we notice that at three non-trivial points the scattering response functions for like spins coincide, $\text{Im}\chi_{\uparrow\uparrow} = \text{Im}\chi_{\downarrow\downarrow}$. Naturally, this is highly sensitive to the effective interactions $V_{\sigma\sigma'}$; in Fig. 4 it occurs at $\hbar\omega/\epsilon_F \approx 1.1, \gtrsim 3, \text{ and } 5$. At these frequencies $\text{Im}\chi_{ns}$ vanishes, the scattering appears paramagnetic.

Third, at $\hbar\omega/\epsilon_F \approx 4.5$, both, $\text{Im}\chi_{\uparrow\downarrow}$ and $\text{Im}\chi_{\uparrow\uparrow}$ vanish. Here, the whole excitation spectrum is given by the response of the minority spin electrons (red solid line in Fig. 4). The frequency $5 \epsilon_F/\hbar$ is particularly interesting, as there the imaginary parts of all three partial response functions became equal. No magnetic resonance is possible, $\text{Im}\chi_{ss} = 0 = \text{Im}\chi_{ns}$. Fig. 4 also shows the smallness and flatness of $\text{Im}\chi_{ss}$ in the vicinity of this zero.

The excitation spectrum for the longitudinal magnetization resulting from $\text{Im}\chi_{ss}$ is shown in Fig. 5 for moderately high (left) and rather low (right) densities (and, again, $N_{\uparrow} \approx 3N_{\downarrow}$). For high r_s the charge plasmon develops a flat region at intermediate wave vectors, related to $S(q)$ there being significantly larger than its RPA counterpart. This implies the considerably lower $q_{\text{pl}}^{\text{max}}$ reported in Table I.

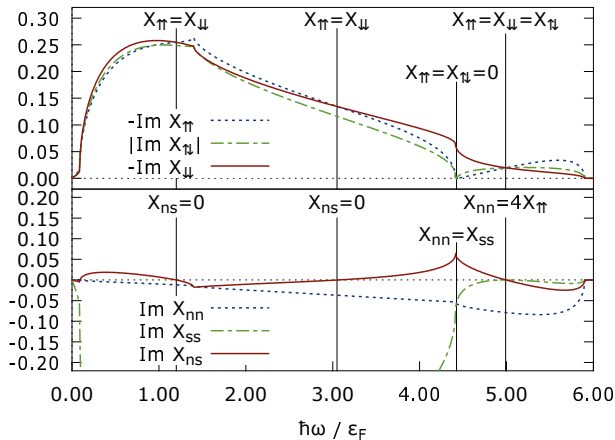


FIG. 4. Comparison of the various excitation domains (see Table II) for $r_s=20$, $P=0.48$ at $q=1.5 k_F$. All response functions are in n/ϵ_F . The charge plasmon is outside the shown range, at $\hbar\omega_{pl} \approx 6.5\epsilon_F$. The vertical lines mark equalities of imaginary parts, the corresponding real parts do not coincide.

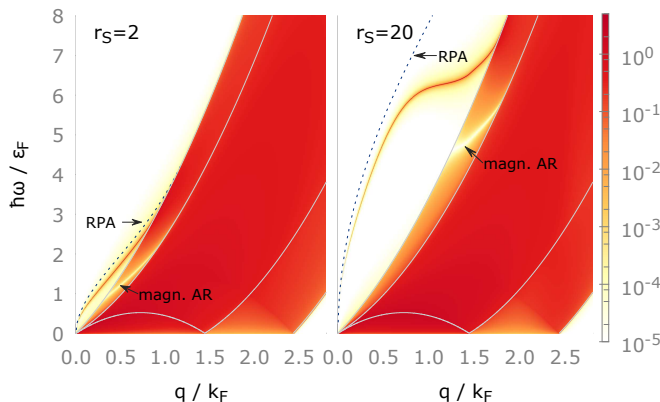


FIG. 5. GRPA imaginary part of the longitudinal spin density response function $-\text{Im} \chi_{ss}(q, \omega)$ (in units $\pi\hbar^2/m$) for two different densities. The grey lines are the characteristic frequencies of the electron-hole continua; the blue dotted line is the RPA charge plasmon. The spin polarization is $P=0.48$.

The longitudinal spin plasmon is too weak to be visible. A prominent feature in Fig. 5 is the white valley around $\omega_{\text{mAR}}(q)$ on the left side of the continua. The physical explanation of this intriguing effect is currently not yet fully clarified. This gap in $\text{Im} \chi_{ss}$ is different from the ‘‘pseudogap’’ found in Ref. 1 for $\text{Im} \epsilon^{-1} \propto \text{Im} \chi_{nn}$.

The antiresonance gap is also present in the bare RPA; the usage of the spin dependent effective potentials of Eq. (8), again, shifts $\omega_{\text{mAR}}(q)$ towards lower energies. We term it ‘‘magnetic antiresonance’’ for the following reason: $\omega_{\text{mAR}}(q)$ does not describe a collective excitation, the real parts of χ_{ss} and χ_{ns} being finite, while the imaginary

parts of both response functions vanish. Therefore, along this line, neither contributions of spin fluctuations δs nor of density fluctuations δn to the double-differential cross section are caused by resonances with a magnetic disturbance b^{ext} . (Conversely, $V^{\text{ext}}(q, \omega_{\text{mAR}}(q))$ does also not cause spin fluctuations in $P \neq 0$ systems). The imaginary part of the permeability determines the magnetic loss in dispersive media³⁶. Although in practical applications transverse precession plays a significant role, the suppression of any dissipation channel is highly desirable. The vanishing of the longitudinal $\text{Im} \chi_{ss}$ around $\omega_{\text{mAR}}(q)$ is therefore very promising. As known for Lorentzian fits of experiments, the maximum in the imaginary part occurs at the resonance frequency, where the real part vanishes. This further supports the name ‘magnetic antiresonance’.

From Fig. 5 it is obvious that the magnetic antiresonance is observed in the particle-hole band of the majority spins. This facilitates the calculation of its dispersion relation. Introducing the dimensionless potential

$$V_{\downarrow+} \equiv \frac{n}{\epsilon_F} (V_{\downarrow\downarrow}(q) + V_{\uparrow\downarrow}(q)), \quad (23)$$

we obtain

$$\frac{\hbar^2 \omega_{\text{mAR}}^2(q)}{\epsilon_{F\downarrow}^2} = \frac{q^2/k_{F\downarrow}^2}{V_{\downarrow+}(q)} \left(2 + V_{\downarrow+}(q)\right)^2 \times \left(\frac{V_{\downarrow+}(q)}{1 + V_{\downarrow+}(q)} + \frac{q^2/k_{F\downarrow}^2}{V_{\downarrow+}(q)}\right). \quad (24)$$

It is straightforward to show that the upper minority spin band is tangentially hit at

$$\frac{2q_{\text{mAR}}^{c\downarrow}}{k_{F\uparrow}} = \frac{V_{\downarrow+}^2}{4(1 + V_{\downarrow+})}, \quad (25)$$

and the upper majority spin band is cut at

$$\frac{2q_{\text{mAR}}^{c\uparrow}}{k_{F\uparrow}} = \frac{V_{\downarrow+}^2 + \sqrt{\frac{2P}{1-P}}(V_{\downarrow+}^2 + 2V_{\downarrow+})}{1 + V_{\downarrow+}}. \quad (26)$$

Both, the spin-spin as well as the density-spin response function take a very simple form along $\omega_{\text{mAR}}(q)$,

$$\chi_{(ns)}^{ss}(q, \omega_{\text{mAR}}(q)) = \frac{1}{(-)} \frac{1}{V_{\uparrow\downarrow}(q)}. \quad (27)$$

The mAR features of the bare RPA are obtained by replacing $V_{\downarrow+}(q)$ with $2nv(q)/\epsilon_F$ in Eqs.(24-27).

In a realistic scattering experiment spin channels have to be taken into account in the double-differential cross section, well explained by Perez³⁷. How exactly the magnetic antiresonance contributes³⁸ to this cross section depends on the size of the optical matrix elements.

IV. CONCLUSION

In summary, we have shown that exchange- and correlation effects substantially alter the response functions

of partially spin-polarized electron layers compared to the bare RPA. In particular, the spin plasmon is shifted downwards and its stability region is severely decreased. For the charge plasmon our results are in good agreement with those obtained from literature-based local field corrections⁵. Finally, we predict a new structure in the double-differential cross section, characterized by a zero in the imaginary part of the spin-spin response function. Certainly, this interesting region and the implications of this effect deserve further research.

ACKNOWLEDGMENTS

We thank Paola Gori-Giorgi for the Quantum Monte Carlo data of the spin-resolved pair-distribution functions with helpful comments and Martin Panholzer for valuable discussions.

-
- ¹ A. Agarwal, M. Polini, G. Vignale, and M. E. Flatté, *Phys. Rev. B* **90**, 155409 (2014).
- ² T. Nagao, T. Hildebrandt, M. Henzler, and S. Hasegawa, *Phys. Rev. Lett.* **86**, 5747 (2001).
- ³ C. F. Hirjibehedin, A. Pinczuk, B. S. Dennis, L. N. Pfeiffer, and K. W. West, *Phys. Rev. B* **65**, 161309 (2002).
- ⁴ S. Moroni, D. M. Ceperley, and G. Senatore, *Phys. Rev. Lett.* **69**, 1837 (1992).
- ⁵ B. Davoudi, M. Polini, G. F. Giuliani, and M. P. Tosi, *Phys. Rev. B* **64**, 153101 (2001).
- ⁶ W. Meevasana, P. King, R. He, S. Mo, M. Hashimoto, A. Tamai, P. Songsiririthigul, F. Baumberger, and Z. Shen, *Nature Materials* **10**, 114 (2011).
- ⁷ A. Santander-Syro, O. Copie, T. Kondo, F. Fortuna, S. Pailhes, R. Weht, X. Qiu, F. Bertran, A. Nicolaou, A. Taleb-Ibrahimi, *et al.*, *Nature* **469**, 189 (2011).
- ⁸ D. Maryenko, J. Falson, Y. Kozuka, A. Tsukazaki, M. Onoda, H. Aoki, and M. Kawasaki, *Phys. Rev. Lett.* **108**, 186803 (2012).
- ⁹ Z. Wang, Z. Zhong, X. Hao, S. Gerhold, B. Stöger, M. Schmid, J. Sánchez-Barriga, A. Varykhalov, C. Franchini, K. Held, *et al.*, *Proceedings of the National Academy of Sciences* **111**, 3933 (2014).
- ¹⁰ X. Hao, Z. Wang, M. Schmid, U. Diebold, and C. Franchini, *Phys. Rev. B* **91**, 085204 (2015).
- ¹¹ T. Gokmen, M. Padmanabhan, E. Tutuc, M. Shayegan, S. De Palo, S. Moroni, and G. Senatore, *Phys. Rev. B* **76**, 233301 (2007).
- ¹² P. Gori-Giorgi, S. Moroni, and G. B. Bachelet, *Phys. Rev. B* **70**, 115102 (2004).
- ¹³ G. Giuliani and G. Vignale, *Quantum theory of the electron liquid* (Cambridge University Press, 2005).
- ¹⁴ F. Stern, *Phys. Rev. Lett.* **18**, 546 (1967).
- ¹⁵ It remains questionable, however, whether this way of packing all non-mean-field effects into dynamic effective potentials optimally elucidates the relevant physics.
- ¹⁶ See, e.g., the references in Ref. 13; and in H. Reinholz and G. Röpke, *Phys. Rev. E* **85**, 036401 (2012).
- ¹⁷ Tanatar, B. and Mutluay, N., *Eur. Phys. J. B* **1**, 409 (1998).
- ¹⁸ D. Neilson, L. Świerkowski, A. Sjölander, and J. Szymański, *Phys. Rev. B* **44**, 6291 (1991).
- ¹⁹ E. H. Hwang and S. Das Sarma, *Phys. Rev. B* **64**, 165409 (2001).
- ²⁰ M. D. Barriga-Carrasco, *Phys. Rev. E* **79**, 027401 (2009) (for bulk systems)
- ²¹ E. Krotscheck, in *Introduction to Modern Methods of Quantum Many-Body Theory*, Vol. 7, edited by A. Fabrocini, S. Fantoni, and E. Krotscheck (World Scientific, Singapore, 2002) pp. 267–330.
- ²² A similar approach was followed for $P=0$ by R. Asgari, A. L. Subaşı, A. A. Sabouri-Dodaran, and B. Tanatar, *Phys. Rev. B* **74**, 155319 (2006) using $V_{\uparrow\uparrow\pm}V_{\uparrow\downarrow}$.
- ²³ E. Krotscheck, *Journal of Low Temperature Physics* **119**, 103 (2000).
- ²⁴ Raw data Monte-carlo data provided by P. Gori-Giorgi.
- ²⁵ M. Polini and M. Tosi, *Many-body physics in condensed matter systems* (Publications of the 0th ed. (Edizioni della Normale, 2006).
- ²⁶ This is also fortunate for spin density functional theory F. G. Eich, S. Pittalis, and G. Vignale, *Phys. Rev. B* **88**, 245102 (2013).
- ²⁷ A. Fetter and J. Walecka, *Quantum Theory of Many-particle Systems*, Dover Books on Physics (Dover Publications, 2003).
- ²⁸ J. Egger, E. Krotscheck, and R. Zillich, *Journal of Low Temperature Physics* **165**, 275 (2011).
- ²⁹ H. M. Böhm, R. Holler, E. Krotscheck, and M. Panholzer, *Phys. Rev. B* **82**, 224505 (2010).
- ³⁰ H. Godfrin, M. Meschke, H.-J. Lauter, A. Sultan, H. M. Böhm, E. Krotscheck, and M. Panholzer, *Nature* **483**, 576 (2012).
- ³¹ Helpful introductions are also found in P. Coleman, *Introduction to Many-Body Physics* (2015) and J. Sólyom, *Fundamentals of the Physics of Solids: Volume 3 - Normal, Broken-Symmetry* (Springer, 2011).
- ³² N. Iwamoto, *Phys. Rev. B* **43**, 2174 (1991).
- ³³ Y. Kwon, D. M. Ceperley, and R. M. Martin, *Phys. Rev. B* **50**, 1684 (1994).
- ³⁴ L. Degiorgi, *Strong interactions in low dimensions*, Vol. 25 (Springer Science & Business Media, 2004).
- ³⁵ We improved the fit of Ref. 12 by removing an unphysical $q \ln q$ -term; ensuring $G(q \rightarrow 0) \propto q$, however, needs further corrections.
- ³⁶ See, ch. 9 in L. D. Landau, *Electrodynamics of continuous media* (Butterworth-Heinemann, Oxford England, 1984).
- ³⁷ F. Perez, *Phys. Rev. B* **79**, 045306 (2009).
- ³⁸ D. Kreil, *Spin-sensitive structure factors and response functions in the* Master's thesis, Johannes Kepler Universität Linz (2014).